Hindawi
International Journal of Antennas and Propagation
Volume 2018, Article ID 2164065, 9 pages
https://doi.org/10.1155/2018/2164065

Research Article

Radiation Pattern Reconfigurable Waveguide Slot Array Antenna Using Liquid Crystal

Hongyu Shi,[1] Jianxing Li,[1] Shitao Zhu,[1] Anxue Zhang,[1] and Zhuo Xu[2]

[1]*School of Electronic and Information Engineering, Xi'an Jiaotong University, Xi'an 710049, China*
[2]*Electronic Materials Research Laboratory, Key Laboratory of the Ministry of Education, Xi'an Jiaotong University, Xi'an 710049, China*

Correspondence should be addressed to Hongyu Shi; honyo.shi1987@gmail.com

Received 9 June 2018; Revised 1 August 2018; Accepted 13 August 2018; Published 9 September 2018

Academic Editor: Shah Nawaz Burokur

In this paper, we proposed a radiation pattern reconfigurable waveguide slot array antenna using liquid crystal (LC). Together with the waveguide slot, the designed complementary electric-field-coupled resonator functions like a switch controlled by the dielectric constant of the LC, which can control the antenna element to radiate or not. Thus, the array factor and radiation pattern can be manipulated. The proposed antenna was simulated, fabricated, and measured. Its radiation direction can be reconfigured to 46° or 0° at about 15 GHz.

1. Introduction

Liquid crystals (LCs) are mixtures in which some degree of anisotropy is present [1]. The nematic phase is one of the most common LC phases. Nematic LCs are uniaxial mediums with an optical axis along the direction of LC molecules or nematic axis. The dielectric constants, measured along ($\varepsilon_{\parallel}$) or normal ($\varepsilon_{\perp}$) to the nematic axis, are different. With a time-dependent external electric field, it is possible to induce a motion in nematic LCs. This motion usually concerns the rotation of the optical axis, which can tune the LC dielectric constant between $\varepsilon_{\parallel}$ and $\varepsilon_{\perp}$ for a certain linearly polarized electromagnetic wave. Such phenomenon is widely used for liquid crystal displays (LCDs), spatial light modulators (SLMs), and reconfigurable electromagnetic wave antennas [2–5] and devices [6–10].

Compared with ferroelectric crystals (e.g., $(Ba,Sr)TiO_3$), the nematic LC has a lower bias voltage, which makes it more suitable for portable reconfigurable electromagnetic wave device design [11–14]. In recent years, nematic LCs have been widely applied for tunable filters [15–18], for tunable phase shifters [19–21], for active metamaterials [22–25], and for frequency [26–28], polarization [21, 29], or radiation pattern reconfigurable [30–35] antennas. Phase shifts of LC phase shifters are usually about 150° and 300° in the microwave [7] and millimetre-wave [36, 37] bands, respectively. Some tunable phase shifters were used in antenna feeding structures to realize polarization or radiation pattern reconfigurable antennas [20, 21]. With a LC substrate, operating frequencies of antennas or frequency selective surfaces can be tuned [4, 27]. LCs were also used to control the reflection phase of grounded structured patches and realize radiation pattern reconfigurable reflect-array antennas from the microwave to submillimetre-wave band [33, 34]. LC-based composite right-/left-handed transmission lines were also designed for radiation pattern reconfigurable leaky wave antennas [24, 31]. These reconfigurable designs are all based on phase shifts resulting from the tunability of LCs' dielectric constants. However, such a method requires continuous bias voltage control and has nonuniform amplitudes for different operating states, which results in a deviation from the practical radiation pattern.

In this paper, a novel method for radiation pattern reconfigurable antenna design using LC was proposed. A nematic LC-loaded metasurface structure was designed. With a bias voltage of 0 V or 30 V for LC, the designed metasurface structure works in the "ON" or "OFF" state like a switch at a certain frequency. This switchable property only

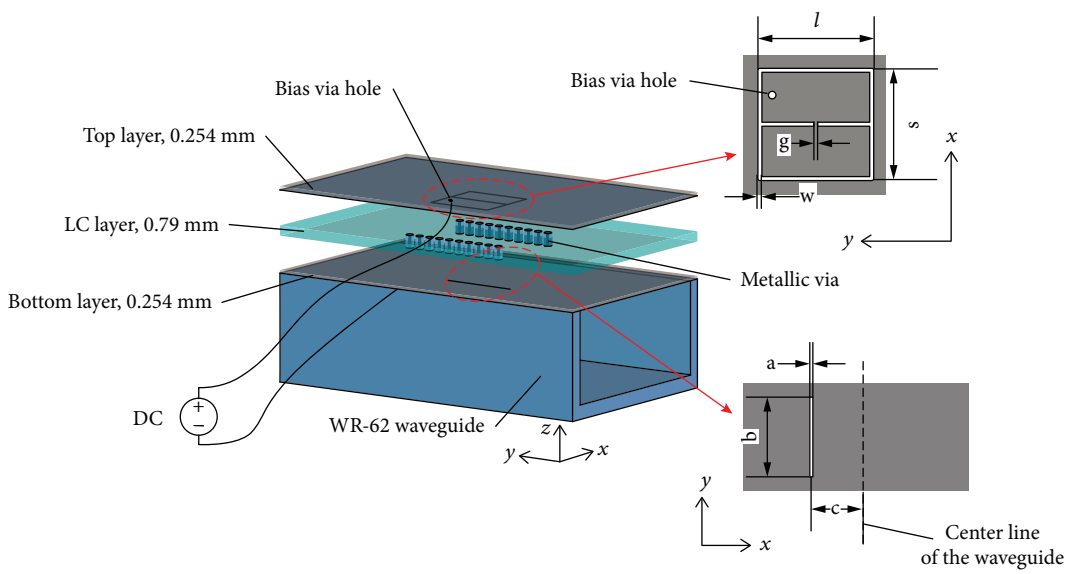

Figure 1: Schematic diagram of the proposed antenna array element.

requires two discrete bias voltages leading to a simpler bias voltage control. By applying the proposed switchable metasurface for a waveguide slot array antenna, the antenna array factor can be controlled, and then the radiation pattern can be steered.

2. Antenna Design

2.1. Antenna Array Element Design. An antenna element was designed to obtain a switchable radiation property. Due to the limited tunability of LC, the designed antenna element should have a narrow bandwidth to avoid bandwidth overlap between each state, which would reduce the radiation pattern reconfiguration property of the waveguide slot array antenna. Thus, an electric-field-coupled resonator-based structure was used, which usually has a narrow bandwidth [38, 39]. The theoretical design rules for such a resonator were proposed in [40, 41].

The proposed slot array element is a multilayered structure including a waveguide slot and a complementary electric-field-coupled (CELC) resonator, as shown in Figure 1. The top layer is metasurface structures with a bias via hole. CELC resonators are closed to the LC layer. The geometric parameters were chosen as $l = 5.7$ mm, $s = 5.5$ mm, $w = 0.2$ mm, and $g = 0.2$ mm. The LC material is LC BNLC1100 provided by the BaYi Space Co. Ltd. The material parameters of LC BNLC1100 are $\varepsilon_{\parallel} = 3.37$, $\varepsilon_{\perp} = 2.6$, $\tan\delta_{\parallel} = 0.014$, and $\tan\delta_{\perp} = 0.022$. The unbiased dielectric constant of unaligned LC BNLC1100 is about 3 to around 15 GHz as measured by Agilent 85070E Dielectric Probe Kit. The thickness of the LC layer is 0.79 mm. The bottom layer is a slot with $a = 0.2$ mm and $b = 6.2$ mm. The slot has an offset of $c = 3.5$ mm from the centre line of the waveguide. The metasurface structure is right above the waveguide slot. The substrate of the top and bottom layers is 0.254 mm thick Taconic RF-60TC with a dielectric constant of 6.15 and a loss tangent of 0.002. The metallic via through the top and LC layers can improve the isolation between each element. The diameter of the metallic via is 0.6 mm. The distance between two adjacent metallic vias is 1 mm. Two columns of the metallic via are located on the middle and edge of the waveguide.

The waveguide slot couples the guided wave from the rectangular waveguide into the LC-loaded metasurface. Then, the CELC resonator above the waveguide slot can be induced. At its resonance frequency, the CELC resonator is excited and radiates like slots. This situation is considered as state "ON" and the electric field distribution in the CELC resonator is shown in Figure 2(a). The slots along the y-direction of the resonator generate x-polarized radiation. However, the electric field in the slots along the x-direction of the resonator are out of phase and cancel each other. Thus, they contribute little to the radiation. At frequencies away from the resonance frequency, the CELC resonator is only slightly induced and almost does not radiate as shown in Figure 2(b). This situation is considered as state "OFF." The resonance frequency can be controlled by changing the dielectric constant of LC. Thus, at a certain frequency, the state of the resonator varies by the dielectric constant of LC.

The antenna element model was built up and simulated by a commercial software CST Microwave Studio. Because the LC bias voltage is loaded along the z-direction, the LC molecules are also along the z-direction. Thus, the LC dielectric constants (ε_{LC}) obtain a lower/higher value for the x-polarized wave radiated from the slot with/without a bias voltage.

Figure 3 shows the S-parameters with different ε_{LC}. The S_{11} parameters are all lower than −15 dB indicating a low reflection of the slot and metasurface structure. The dips of the S_{21} parameters are caused by the radiation of the structure. The radiation frequency goes higher with a smaller ε_{LC}. When $\varepsilon_{LC} = 3$, the S_{21} parameter is −1.64 dB at 15 GHz, which would be much lower using multiple elements

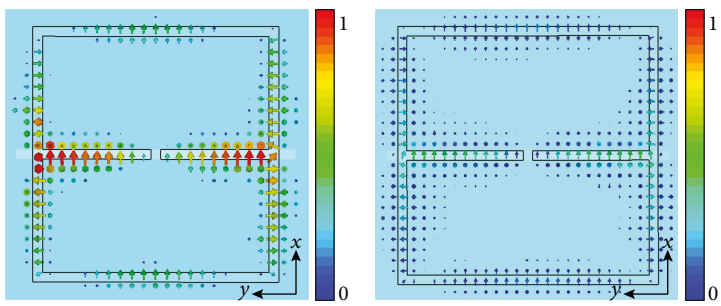

Figure 2: Electric field distributions for the CELC resonator: (a) state "ON," (b) state "OFF."

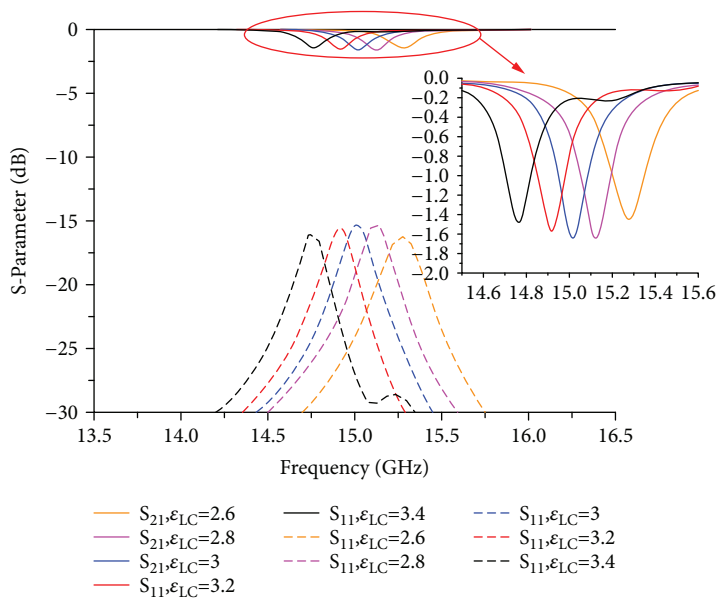

Figure 3: Simulated S-parameters of the antenna element with different ε_{LC}.

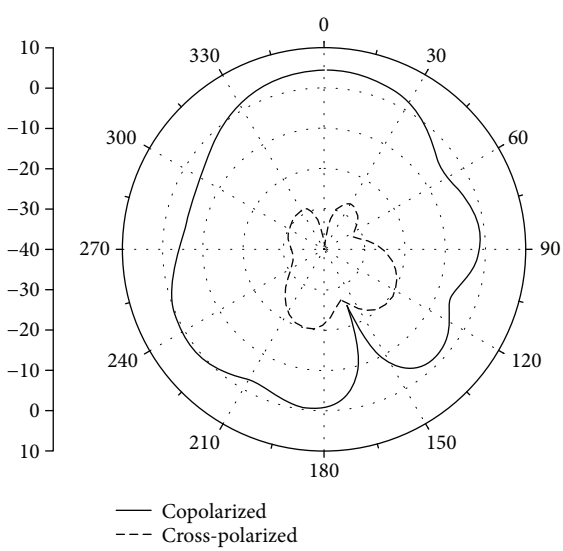

Figure 4: Simulated radiation pattern of the antenna element.

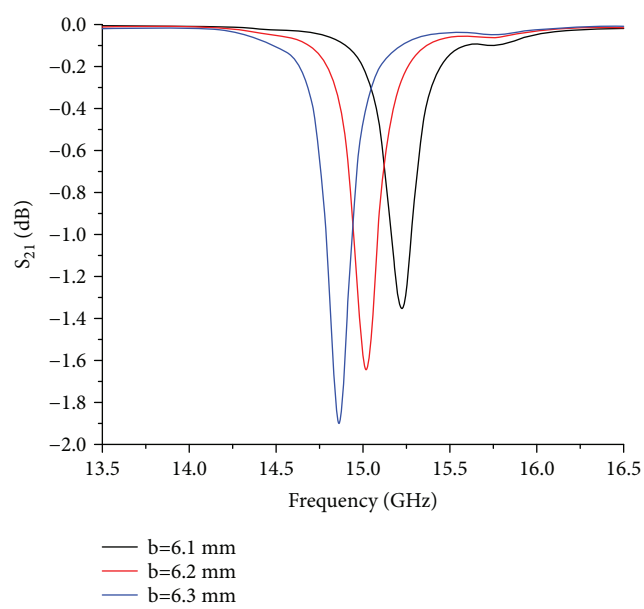

Figure 5: Simulated S_{21} parameters with different b.

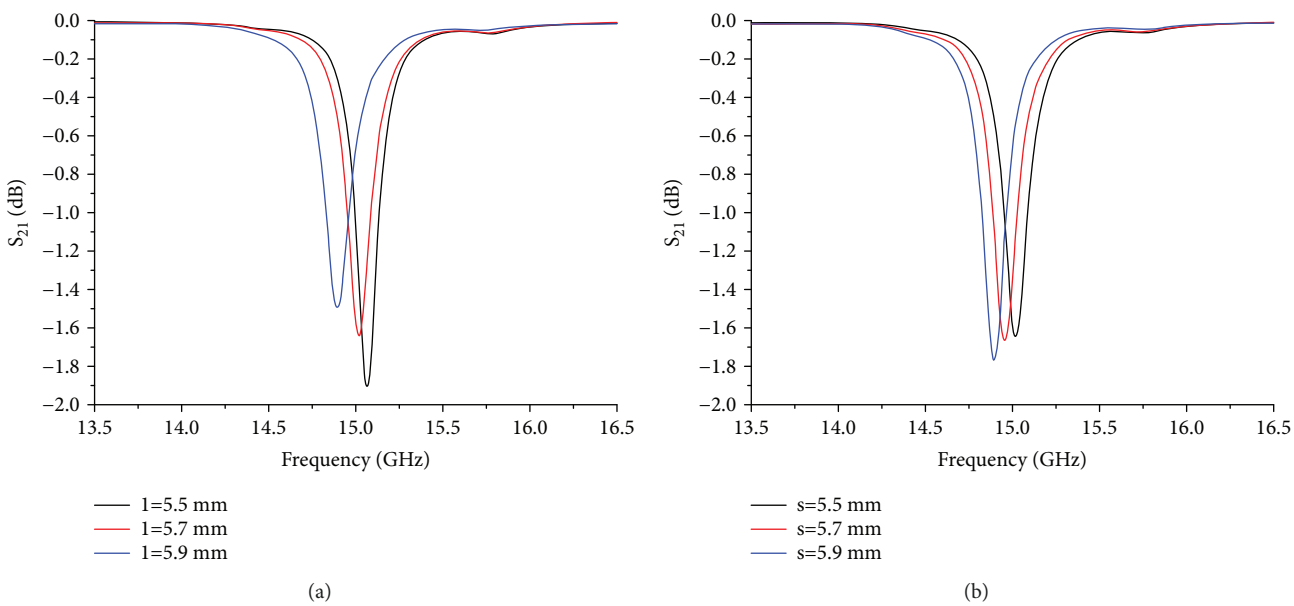

Figure 6: Simulated S_{21} parameters with different (a) l and (b) s.

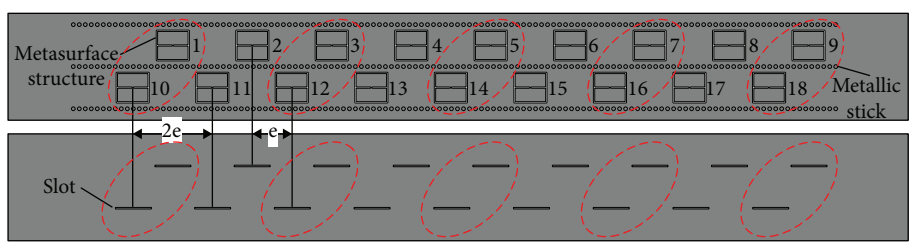

Figure 7: Element arrangement of the proposed waveguide slot array antenna.

as an array. When ε_{LC} is greater or lower than 3, the S_{21} parameter is higher at 15 GHz. For example, when ε_{LC} is 3.4 or 2.6, the S_{21} parameter is higher than −0.2 dB at 15 GHz, which means the radiated power is much lower. Thus, around 15 GHz, when the difference between ε_{LC} with and without bias is higher than 0.4, the antenna element can function like a switch controlled by a bias voltage.

The radiation pattern of the antenna element with $\varepsilon_{LC} = 3$ in the *yoz* plane is shown in Figure 4. The antenna element is *x*-polarized, and the plane of polarization is the *xoz* plane. The copolarized gain is 4.46 dB, and the cross-polarized gain is below −38 dB. The width of the main lobe is about ±30°.

A parameter studies for key geometric parameters of the antenna element are shown in Figures 5 and 6. As shown in Figure 5, with a bigger b, the resonance frequency has a red shift and S_{21} becomes lower, which means more power is leaked. As shown Figure 6(a), with a bigger l, the resonance frequency become lower and less power is leaked. s has a smaller impact on the resonance frequency. A bigger s leads to a slightly lower resonance frequency. Resonators with different geometric parameters have different resonance frequencies. However, at their resonance frequencies, the radiation patterns are similar due to the same resonant mode.

2.2. Waveguide Slot Array Antenna Design. The used rectangular waveguide is WR62 operating from 11.9 GHz to 18 GHz. The proposed antenna contains 18 longitudinal slots as shown in Figure 7. The distance between each slot is $e = \lambda_g/4 = 6.6$ mm, where λ_g is the guide wavelength at 15 GHz. Thus, the feeding phase difference for adjacent elements is $\xi = 90^\circ$.

As mentioned above, the metasurface structure with LC functions like a switch with different bias voltages, which controls the antenna element from radiating or not. Thus, the arrangement of the slot array or the array factor can be controlled by the bias voltage, and then the radiation pattern can be steered in the *yoz* plane.

The normalized array factor is

$$|A(\psi)| = \frac{1}{N}\left|\frac{\sin(N\psi/2)}{\sin(\psi/2)}\right|, \quad (1)$$

where

$$\psi = \beta d \cos\phi + \xi. \quad (2)$$

β is the wavenumber in the vacuum, d is the distance between each radiating element, and ϕ is the observation

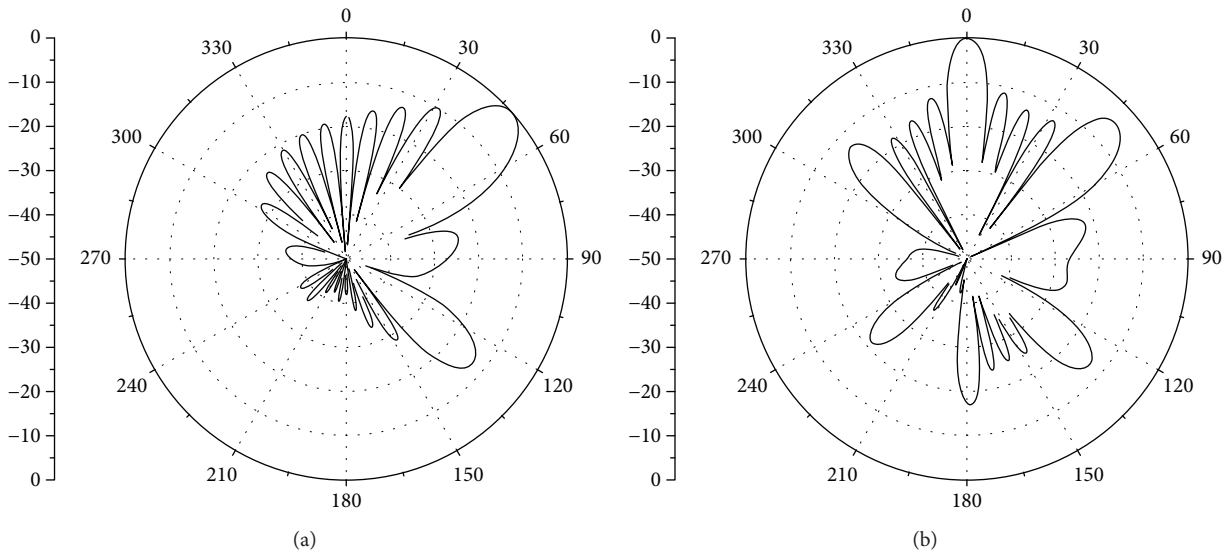

Figure 8: Calculated radiation pattern for (a) Configuration 1 and (b) Configuration 2.

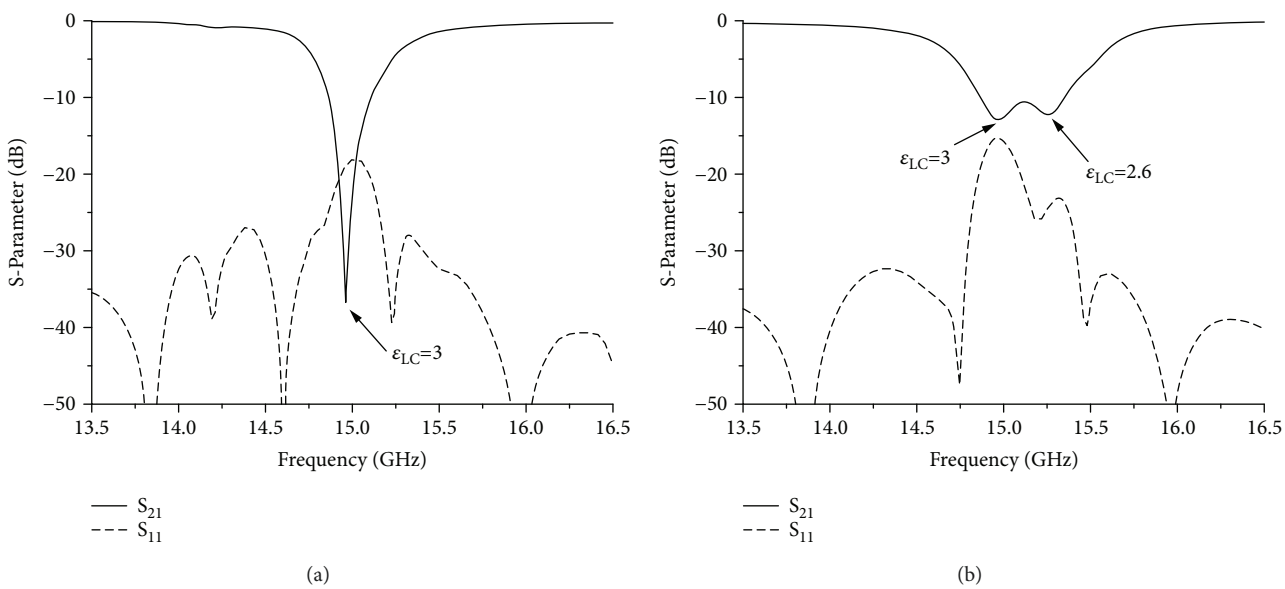

Figure 9: Simulated S-parameters of the antenna arrays: (a) Configuration 1; (b) Configuration 2.

angle. When all the antenna elements are radiating, the waveguide slot array antenna is a uniform linear array (Configuration 1) with $d = e = 6.6$ mm and $\xi = 90^\circ$. When only nos. 1, 3, 5, 7, 9, 10, 12, 14, 16, and 18 of these elements are radiating, considering each adjacent two slots as one element (red circled), the waveguide slot array antenna is a five-element array (Configuration 2) with a distance between each element of $d = 4e = 26.4$ mm and $\xi = 0^\circ$. The calculated radiation pattern for these two slot arrays in the *yoz* plane are shown in Figures 8(a) and 8(b). The plane of polarization is the *xoz* plane. The main lobe directions for Configuration 1 and Configuration 2 are 48° and 0°, respectively. The grating lobe is caused by the relative big distance between each element.

3. Simulation and Measurement Results

The designed waveguide slot array antenna was simulated by CST Microwave Studio. The simulated S-parameters of the Configuration 1 and Configuration 2 (as described in the previous section) are shown in Figures 9(a) and 9(b). The S_{11} parameters are lower than −15 dB. The S_{21} parameter of the Configuration 1 has only one dip of −36.8 dB at 14.96 GHz with $\varepsilon_{LC} = 3$ for all the elements. However, for the Configuration 2, the S_{21} parameter has two dips of −12.88 dB and −12.23 dB at 14.97 GHz and 15.26 GHz, respectively. The lower and upper dips are caused by the antenna elements operating in two states with $\varepsilon_{LC} = 3$ and $\varepsilon_{LC} = 2.6$, respectively. These transmission dips indicate the

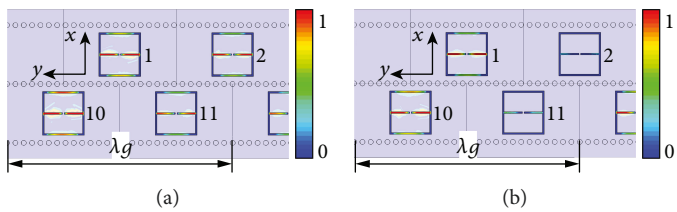

Figure 10: Simulated x component of electric field distributions: (a) Configuration 1; (b) Configuration 2.

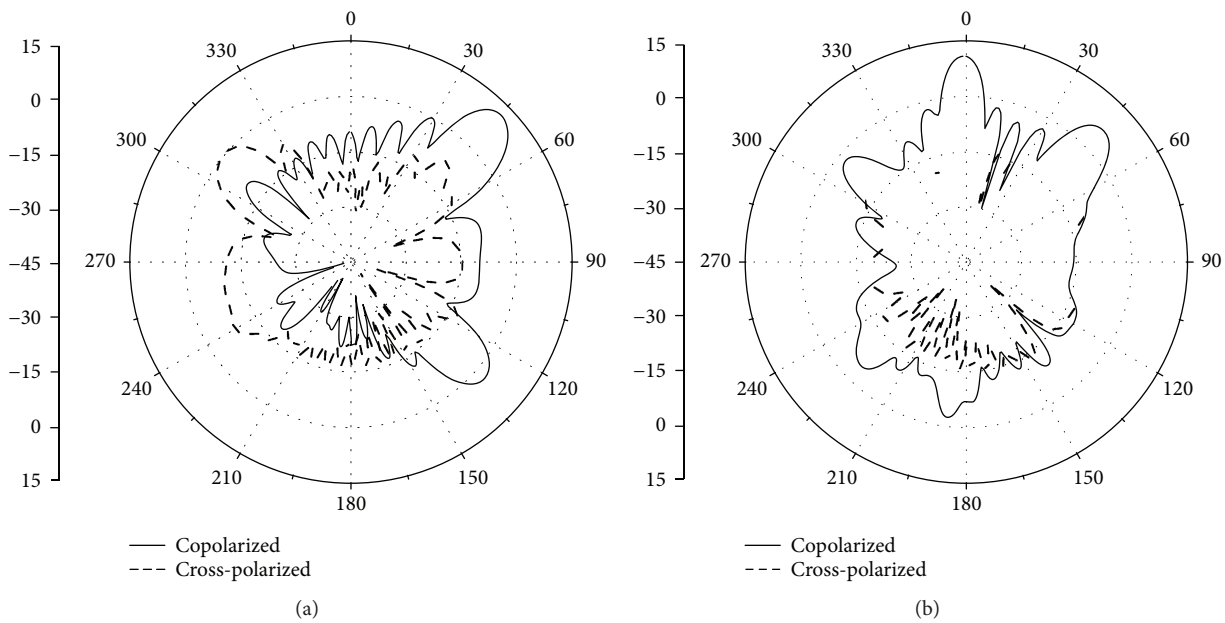

Figure 11: Simulated radiation patterns of the antenna arrays: (a) Configuration 1; (b) Configuration 2.

radiation of the waveguide slot array antenna. In this paper, we focus on the radiation characteristics in the *yoz* plane at about 15 GHz.

The simulated electric field distributions of the waveguide slot array antenna within one wavelength are shown in Figure 10. The field distributions of other parts of the array antenna are similar. E_x-field distribution for Configuration 1 is shown in Figure 10(a). With $\varepsilon_{LC} = 3$, all the elements are excited. However, as for the Configuration 2, only the elements with $\varepsilon_{LC} = 3$ (nos. 1, 10, etc.) are excited and the elements with $\varepsilon_{LC} = 2.6$ (nos. 2, 11, etc.) are not excited as shown in Figure 10(b). Thus, by controlling the ε_{LC}, the array factor of the waveguide slot array antenna can be controlled and the radiation pattern can be reconfigured.

Figures 11(a) and 11(b) show the radiation patterns for Configuration 1 and Configuration 2, respectively, at 14.96 GHz. The array antenna is x-polarized, and the plane of polarization is the *xoz* plane. The main lobe directions of Configuration 1 and Configuration 2 are about 46° and 0°, respectively, with copolarized gains of 11.7 dB and 10.68 dB. The cross-polarized gains of Configuration 1 and Configuration 2 are −21.61 dB and −8.28 dB at 14.96 GHz. Thus, by controlling the LC bias voltage, radiation pattern of the proposed waveguide slot array antenna is reconfigurable. The grating lobe levels of Configuration 1 and Configuration 2 are −8.6 dB and − 4.21 dB, respectively. As described in the previous section, the grating lobe of Configuration 2 is caused by the relative big distance between the radiating elements.

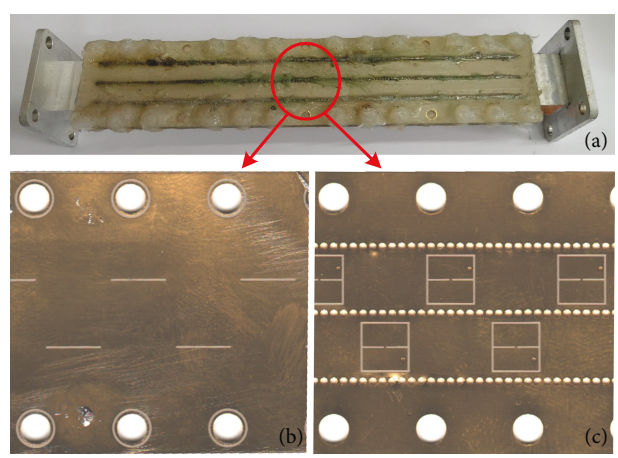

Figure 12: Photos of the fabricated sample. (a) waveguide slots array antenna, (b) slot layer, (c) metasurface layer.

The proposed reconfigurable waveguide slot array antenna was fabricated and measured for further demonstration. The photos of the fabricated sample are shown in Figure 12(a). Figures 12(b) and 12(c) show the detail

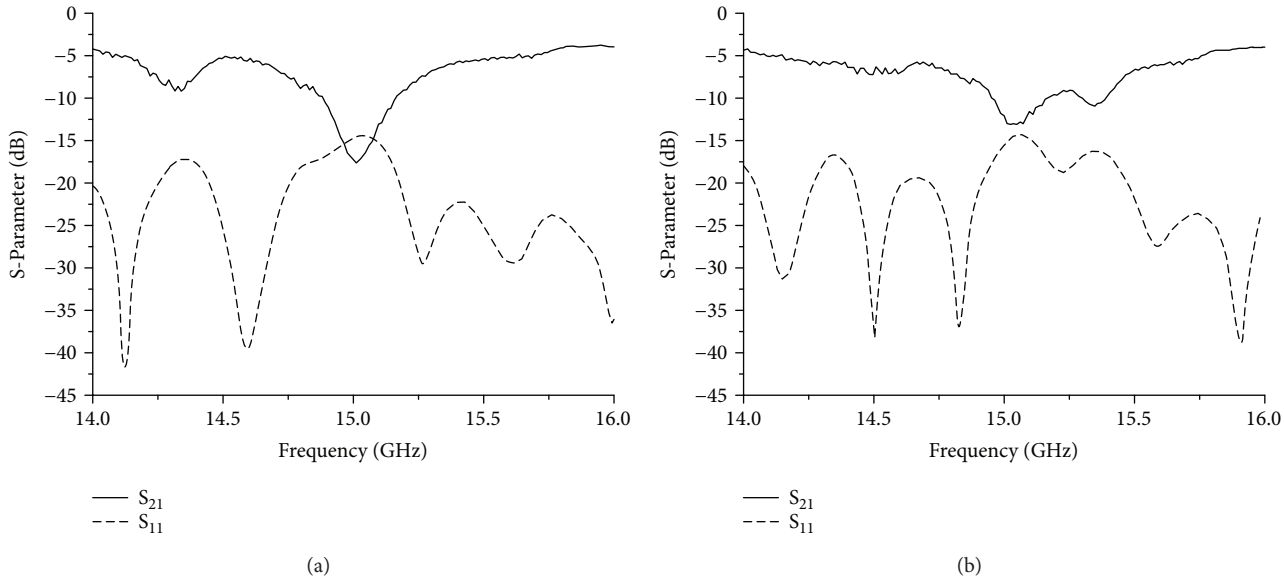

Figure 13: The fabricated sample and measured S-parameters of the antenna arrays: (a) Configuration 1; (b) Configuration 2.

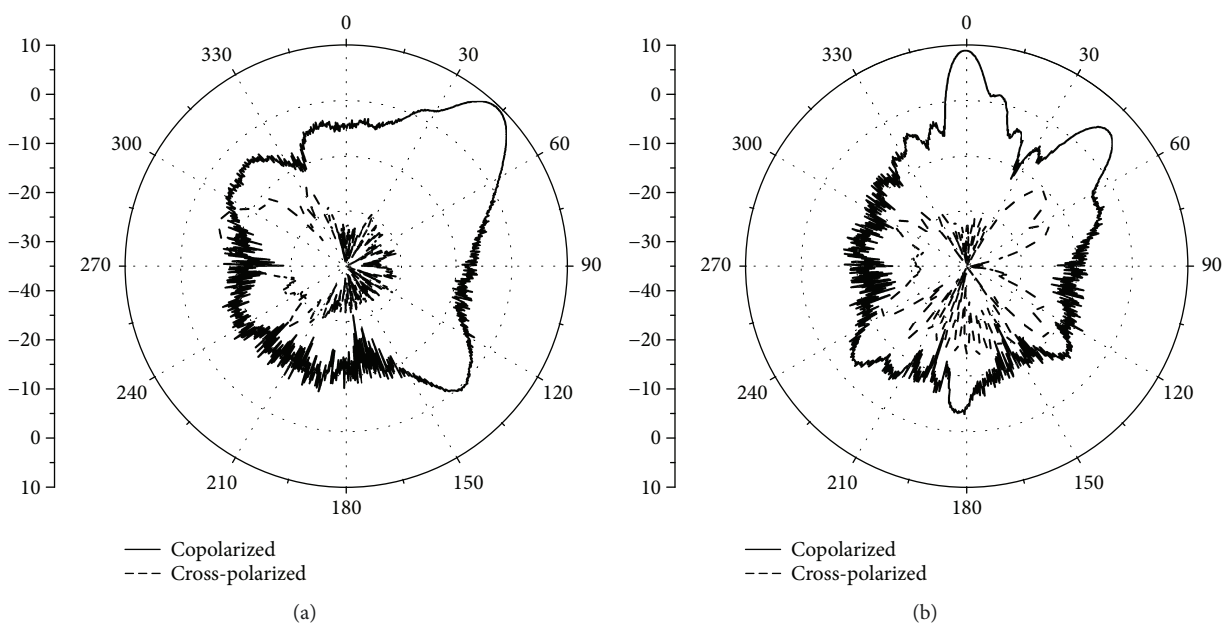

Figure 14: Measured radiation patterns of the antenna arrays: (a) Configuration 1; (b) Configuration 2.

structure of the slots and CELC resonators. The holes on the upper and lower sides are used for assembly. The measured S-parameters confirm with the simulation results. The LC is unaligned, and the initial ε_{LC} is 3 as aforementioned. Two antenna states were measured. The first state is unbiased, and all the antenna elements are radiating. The second state has a bias voltage of 30 V on the red circled elements in Figure 7, and these elements are not radiating. After being biased with a 30 V DC voltage, the property of the sample trended to be stable after 7 minutes, which can be reduced by using a thinner LC layer. The fabricated antenna sample was measured by a vector network analyser of Agilent E8363b, and the bias network was fed by a DC source of Motech LPS-305.

The measured S-parameter and radiation pattern are shown in Figures 13 and 14, respectively. As shown in Figure 13(a), Configuration 1 is unbiased; at 15.01 GHz, the S_{11} parameter is lower than −14.5 dB and the S_{21} parameter is −17.67 dB. As for Configuration 2, the S_{11} parameter is below −15 dB, and the S_{21} parameter has two dips of −13.09 dB and −10.93 dB at 15.04 GHz and 15.35 GHz, respectively. At 15.04 GHz, the S_{21} parameter of Configuration 1 is −16.8 dB. As shown in Figure 14, the main lobe directions of Configuration 1 and Configuration 2 are 44° and 0°, respectively, with gains of 9.81 dB and 9.02 dB. The cross-polarized gains of Configuration 1 and Configuration 2 are below −20 dB. The grating lobe level of Configuration 1 and Configuration 2 is −9.17 dB and

−3.62 dB, respectively. The plane of polarization is the *xoz* plane. Thus, the measurement radiation patterns confirm with the simulation results, and the differences are caused by the mechanical errors and measurement errors. By controlling the bias voltage on LC, the array factor can be controlled and a radiation pattern reconfigurable waveguide slot array antenna was realized.

4. Conclusions

In conclusion, using LC material, a switchable antenna element with a tuneable radiation power was designed. An 18-element waveguide slot array antenna was then proposed. By controlling the LC bias voltage, the array factor and the radiation pattern can be controlled. Two situations were demonstrated by both simulation and measurement. For these two situations, the measured radiation directions are 44° and 0° and the measured gains are 9.81 dB and 9.02 dB at 15.04 GHz. The grating lobe can be suppressed by reducing the distance between each element using transverse slot array antenna, which also has potentials for more beam-steering configurations. The side lobs can be suppressed by using a Chebyshev array antenna.

Data Availability

(1) The plot data of the array factor used to support the mechanism of this study are included within the article. (2) The plot data of reconfigurable radiation patterns used to support the conclusion of this study are included within the article.

Conflicts of Interest

The authors declare that they have no conflicts of interest.

Acknowledgments

This work was supported in part by the National Natural Science Foundation of China (NSFC) (61501365, 61471292, and 61331005) and China Postdoctoral Science Foundation (CPSF) (2015M580849).

References

[1] P. G. D. Gennes and J. Prost, *The Physics of Liquid Crystals*, Clarendon Press, Oxford University Press, Oxford, New York, 2nd edition, 1993.

[2] P. Deo, D. Mirshekar-Syahkal, L. Seddon, S. E. Day, and F. A. Fernandez, "Microstrip device for broadband (15-65 GHz) measurement of dielectric properties of nematic liquid crystals," *IEEE Transactions on Microwave Theory and Techniques*, vol. 63, no. 4, pp. 1388–1398, 2015.

[3] W. Hu, M. Y. Ismail, R. Cahill et al., "Liquid-crystal-based reflectarray antenna with electronically switchable monopulse patterns," *Electronics Letters*, vol. 43, no. 14, pp. 744-745, 2007.

[4] W. Hu, R. Dickie, R. Cahill et al., "Liquid crystal tunable mm wave frequency selective surface," *IEEE Microwave and Wireless Components Letters*, vol. 17, no. 9, pp. 667–669, 2007.

[5] L. Liu and R. J. Langley, "Liquid crystal tunable microstrip patch antenna," *Electronics Letters*, vol. 44, no. 20, pp. 1179–1181, 2008.

[6] O. H. Karabey, A. Gaebler, S. Strunck, and R. Jakoby, "A 2-D electronically steered phased-array antenna with 2 x 2 elements in LC display technology," *IEEE Transactions on Microwave Theory and Techniques*, vol. 60, no. 5, pp. 1297–1306, 2012.

[7] Y. Utsumi, T. Kamei, K. Saito, and H. Moritake, "Increasing the speed of microstrip-line-type polymer-dispersed liquid-crystal loaded variable phase shifter," *IEEE Transactions on Microwave Theory and Techniques*, vol. 53, no. 11, pp. 3345–3353, 2005.

[8] N. Tentillier, F. Krasinski, R. Sauleau, B. Splingart, H. Lhermite, and P. Coquet, "A liquid-crystal, tunable, ultra-thin Fabry-Perot resonator in Ka band," *IEEE Antennas and Wireless Propagation Letters*, vol. 8, no. 8, pp. 701–704, 2009.

[9] F. Zhang, W. Zhang, Q. Zhao et al., "Electrically controllable fishnet metamaterial based on nematic liquid crystal," *Optics Express*, vol. 19, no. 2, pp. 1563–1568, 2011.

[10] Y. Garbovskiy, V. Zagorodnii, P. Krivosik et al., "Liquid crystal phase shifters at millimeter wave frequencies," *Journal of Applied Physics*, vol. 111, no. 5, article 054504, 2012.

[11] M. Nikfalazar, M. Sazegar, A. Mehmood et al., "Two-dimensional beam-steering phased-array antenna with compact tunable phase shifter based on BST thick films," *IEEE Antennas and Wireless Propagation Letters*, vol. 16, pp. 585–588, 2017.

[12] H. Park, F. Fan, M. Lim, H. Han, V. G. Chigrinov, and E. MacPherson, "Terahertz properties of liquid crystals," in *2011 International Conference on Infrared, Millimeter, and Terahertz Waves*, Houston, TX, USA, October 2011.

[13] S. Mueller, M. Koeberle, F. Goelden et al., "W-Band characterization of anisotropic liquid crystals at room temperature," in *2008 38th European Microwave Conference*, pp. 119–122, Amsterdam, Netherlands, October 2008.

[14] S. Mueller, A. Penirschke, C. Damm et al., "Broad-band microwave characterization of liquid crystals using a temperature-controlled, coaxial transmission line," *IEEE Transactions on Microwave Theory and Techniques*, vol. 53, no. 6, pp. 1937–1945, 2005.

[15] M. Yazdanpanahi and D. Mirshekar-Syahkal, "Millimeter-wave liquid-crystal-based tunable bandpass filter," in *2012 IEEE Radio and Wireless Symposium*, pp. 139–142, Santa Clara, CA, USA, January 2012.

[16] J. Torrecilla, E. Avila-Navarro, C. Marcos et al., "Microwave tunable notch filter based on liquid crystal using spiral spurline technology," *Microwave and Optical Technology Letters*, vol. 55, no. 10, pp. 2420–2423, 2013.

[17] Y. Liu, D. Jiang, L. Xia, and R. Xu, "A novel microwave tunable band-pass filter integrated power divider based on liquid crystal," *International Journal of Antennas and Propagation*, vol. 2015, Article ID 320910, 6 pages, 2015.

[18] T. Franke, R. Jakoby, M. Nickel et al., "Continuously tunable substrate integrated waveguide bandpass filter in liquid crystal technology with magnetic biasing," *Electronics Letters*, vol. 51, no. 20, pp. 1584-1585, 2015.

[19] A. L. Franc, O. H. Karabey, G. Rehder, E. Pistono, R. Jakoby, and P. Ferrari, "Compact and broadband millimeter-wave electrically tunable phase shifter combining slow-wave effect with liquid crystal technology," *IEEE Transactions on*

Microwave Theory and Techniques, vol. 61, no. 11, pp. 3905–3915, 2013.

[20] R. Cahill, N. Mitchell, A. Manabe, S. Christie, and Y. Munro, "Electronically scanned Rotman lens antenna with liquid crystal phase shifters," *Electronics Letters*, vol. 49, no. 7, pp. 445–447, 2013.

[21] O. H. Karabey, S. Bildik, S. Bausch, S. Strunck, A. Gaebler, and R. Jakoby, "Continuously polarization agile antenna by using liquid crystal-based tunable variable delay lines," *IEEE Transactions on Antennas and Propagation*, vol. 61, no. 1, pp. 70–76, 2013.

[22] D. C. Zografopoulos and R. Beccherelli, "Tunable terahertz fishnet metamaterials based on thin nematic liquid crystal layers for fast switching," *Scientific Reports*, vol. 5, no. 1, article 13137, 2015.

[23] N. Chikhi, M. Lisitskiy, G. Papari, V. Tkachenko, and A. Andreone, "A hybrid tunable THz metadevice using a high birefringence liquid crystal," *Scientific Reports*, vol. 6, no. 1, article 34536, 2016.

[24] B. J. Che, T. Jin, D. Erni, F. Y. Meng, Y. L. Lyu, and Q. Wu, "Electrically controllable composite right/left-handed leaky-wave antenna using liquid crystals in PCB technology," *IEEE Transactions on Components, Packaging and Manufacturing Technology*, vol. 7, no. 8, pp. 1331–1342, 2017.

[25] M. Maasch, M. Roig, C. Damm, and R. Jakoby, "Voltage-tunable artificial gradient-index lens based on a liquid crystal loaded fishnet metamaterial," *IEEE Antennas and Wireless Propagation Letters*, vol. 13, pp. 1581–1584, 2014.

[26] Y. Zhao, C. Huang, A.-Y. Qing, and X. Luo, "A frequency and pattern reconfigurable antenna array based on liquid crystal technology," *IEEE Photonics Journal*, vol. 9, no. 3, pp. 1–7, 2017.

[27] M. A. Christou, N. C. Papanicolaou, and A. C. Polycarpou, "Frequency-agile microstrip patch antenna on a biased liquid crystal substrate," *Electronics Letters*, vol. 51, no. 3, pp. 202–204, 2015.

[28] A. C. Polycarpou, M. A. Christou, and N. C. Papanicolaou, "Tunable patch antenna printed on a biased nematic liquid crystal cell," *IEEE Transactions on Antennas and Propagation*, vol. 62, no. 10, pp. 4980–4987, 2014.

[29] O. H. Karabey, S. Bildik, S. Strunck, A. Gaebler, and R. Jakoby, "Continuously polarisation reconfigurable antenna element by using liquid crystal based tunable coupled line," *Electronics Letters*, vol. 48, no. 3, pp. 141-142, 2012.

[30] G. Xu, H.-L. Peng, C. Sun, J.-G. Lu, Y. Zhang, and W.-Y. Yin, "Differential probe fed liquid crystal-based frequency tunable circular ring patch antenna," *IEEE Access*, vol. 6, pp. 3051–3058, 2018.

[31] M. Roig, M. Maasch, C. Damm, and R. Jakoby, "Investigation and application of a liquid crystal loaded varactor in a voltage tunable CRLH leaky-wave antenna at Ka-band," *International Journal of Microwave and Wireless Technologies*, vol. 7, no. 3-4, pp. 361–367, 2015.

[32] B. J. Che, F. Y. Meng, Y. L. Lyu, and Q. Wu, "Reconfigurable dual-band metamaterial antenna based on liquid crystals," *Journal of Physics D-Applied Physics*, vol. 51, no. 18, article 185102, 2018.

[33] G. Perez-Palomino, M. Barba, J. A. Encinar et al., "Design and demonstration of an electronically scanned reflectarray antenna at 100 GHz using multiresonant cells based on liquid crystals," *IEEE Transactions on Antennas and Propagation*, vol. 63, no. 8, pp. 3722–3727, 2015.

[34] S. Bildik, S. Dieter, C. Fritzsch, W. Menzel, and R. Jakoby, "Reconfigurable folded reflectarray antenna based upon liquid crystal technology," *IEEE Transactions on Antennas and Propagation*, vol. 63, no. 1, pp. 122–132, 2015.

[35] C. M. Watts, A. Pedross-Engel, D. R. Smith, and M. S. Reynolds, "X-band SAR imaging with a liquid-crystal-based dynamic metasurface antenna," *Journal of the Optical Society of America B*, vol. 34, no. 2, pp. 300–306, 2017.

[36] J. F. Li, H. Xu, and D. P. Chu, "Design of liquid crystal based coplanar waveguide tunable phase shifter with no floating electrodes for 60–90 GHz applications," in *2016 46th European Microwave Conference (EuMC)*, pp. 1047–1050, London, UK, October 2016.

[37] C. Fritzsch, M. Jost, O. H. Karabey et al., "Liquid crystal based low-loss phase shifter for W-band frequencies," *Electronics Letters*, vol. 49, no. 23, pp. 1460–1462, 2013.

[38] H. Shi, A. Zhang, S. Zheng, J. Li, and Y. Jiang, "Dual-band polarization angle independent 90° polarization rotator using twisted electric-field-coupled resonators," *Applied Physics Letters*, vol. 104, no. 3, article 034102, 2014.

[39] H. Shi, J. Li, A. Zhang et al., "Gradient Metasurface with both polarization-controlled directional surface wave coupling and anomalous reflection," *IEEE Antennas and Wireless Propagation Letters*, vol. 14, pp. 104–107, 2015.

[40] T. H. Hand, J. Gollub, S. Sajuyigbe, D. R. Smith, and S. A. Cummer, "Characterization of complementary electric field coupled resonant surfaces," *Applied Physics Letters*, vol. 93, no. 21, article 212504, 2008.

[41] P. Pushkar and V. R. Gupta, "A design rule for an ELC resonator," in *2015 International Conference on Innovations in Information, Embedded and Communication Systems (ICIIECS)*, pp. 1–4, Coimbatore, India, March 2015.